Oil & Natural Gas Technology

DOE Award No.: DE-FC26-06NT43067

Quarterly Progress Report
(April – June 2011)

Mechanisms Leading to Co-Existence of Gas and Hydrate in Ocean Sediments

Submitted by:
The University of Texas at Austin
1 University Station C0300
Austin, TX 78712-0228

Prepared for:
United States Department of Energy
National Energy Technology Laboratory

July 26, 2011

Office of Fossil Energy

MECHANISMS LEADING TO CO-EXISTENCE OF GAS AND HYDRATE IN OCEAN SEDIMENTS

CONTRACT NO. DE-FC26-06NT43067

QUARTERLY PROGRESS REPORT
Reporting Period: 1 Apr 11 – 30 Jun 11

Prepared by

Steven L. Bryant
Department of Petroleum and Geosystems Engineering
The University of Texas at Austin
1 University Station C0300
Austin, TX 78712-0228
Phone: (512) 471 3250
Email: steven_bryant@mail.utexas.edu

Ruben Juanes
Department of Civil and Environmental Engineering
Massachusetts Institute of Technology
77 Massachusetts Avenue, Room 48-319
Cambridge, MA 02139
Phone: (617)253-7191
Email: juanes@mit.edu

Prepared for
U.S. Department of Energy - NETL
3610 Collins Ferry Road
P.O. Box 880
Morgantown, WV 26508

Acknowledgment: "This material is based upon work supported by the Department of Energy under Award Number DE-FC26-06NT43067."

Summary

A mechanistic model is developed to explain/predict gas hydrate saturation profile in sub-permafrost formations in the Arctic. The model assumes that the gas hydrate profiles are converted free gas accumulations when base of gas hydrate stability zone (BGHSZ) moves down the gas column. Three key elements are considered in the model: (1) volume change during hydrate formation and consequent fluid phase transport; (2) the descent of BGHSZ through the column and (3) sedimentological (i.e. grain size) variation with depth. The model shows that substantial amount of fluid (of order of one pore volume of aqueous and/or gaseous phase) must have migrated within or into the gas column during hydrate formation. Moreover, evaluation of typical relative permeability curves and fractional flow theory shows that due to the very low mobility ratio of aqueous to gas phase, the amount of water required during hydrate formation, $\Delta V_{w,d}$, cannot be transported through a co-current type of flow. It is rather another type of flow, i.e. water is transported from above into the hydrate formation zone and gas is being provided from the lower free gas column. The model matches the hydrate saturation distribution from Mt. Elbert well in the Alaskan North Slope if the volume of gas that migrated within the column is approximately equal to the volume of water that migrated into the column.

Activities in This Reporting Period

Task 8.0 - Modeling methane transport at the bed scale

Subtask 8.1 Application of bed-scale model to sub-permafrost hydrate accumulations

Background and Review of Previous Results. Evaluation of gas hydrates deposits has recently begun to adopt the perspective of petroleum systems analysis [1-3]. The analysis is complicated by the different possible modes of charging a hydrate accumulation. Hydrate occurs in various morphologies (pore filling, fracture filling, etc.) and in various bed-scale distributions of saturation among and within hydrate provinces. Sediment inhibits gas hydrate nucleation and growth compared to free-phase [4], [5]. As a result of such observations and relevant models proposed in the literature [6], [7], the preferential accumulation of gas hydrate in coarse-grained rather than fine-grained layers of sediment is now part of conventional wisdom.

Efforts to explain the bed-scale distribution can be divided into two main categories: (A) hydrate forms from methane dissolved in water and accumulation is driven by methane-saturated water entering the gas hydrate stability zone (GHSZ)[8-13] and (B) hydrate forms at the interface between gaseous and aqueous phases and accumulation is driven by methane gas phase entering the GHSZ [14-17]. One motivation for the latter class of models was that observed chloride concentrations and gas hydrate distributions at the southern summit of Hydrate Ridge could not be explained without assuming transport of free gas through GHSZ [14].

Observations of hydrate that only partially fills coarse-grained layers, as reported for the Mt. Elbert test well [18], cannot be explained by either category of model. We have argued [19] that this type of hydrate occurrence is consistent with three conditions: i) the establishment of gas phase saturation within the sediment when the base of gas hydrate stability zone (BGHSZ) was located above the sediment package; ii) sufficient variation of grain size distribution with depth and iii) temperature and pressure conditions such that hydrate occupies less volume than its constituents (CH_4, H_2O) in their respective phases. If the base of GHSZ then moves to (and through) the initially static fluid phases, for example due to cooling at the surface, the accumulated gas in the sediment (and some of the water) can be converted to hydrate. The first condition has been satisfied in Arctic sediments over geologic time. The second condition depends on local depositional history. The third condition is satisfied for a range of sediment depths when permafrost exists in shallower sediments.

In this model the conversion of gas to hydrate proceeds from top to bottom of the gas accumulation. If the accumulation is no longer connected to the source of the charge, then the fluid volume reduction associated with hydrate formation at the top of the accumulation will cause the gas/water contact to rise at the bottom of the accumulation. The capillary pressure of the gas phase remaining in the column thus decreases. This can lead to disconnection of the gas accumulation at layers having larger-than-average capillary entry pressure. The result is a hydrate saturation profile that differs qualitatively and quantitatively from the original gas saturation profile in the sediment column [19].

In this report we summarize several elements of this model and then discuss an important new implication of the model: **large volumes of fluid phases must move within the original gas accumulation, and into the sediment hosting the gas accumulation**. Because the fluid volumes are large, we assume here that the alternative to fluid movement, which is compaction or grain rearrangement within the sediment, can be neglected. We also assume that methane that moves to the GHSZ is subsequently converted to hydrate. We assume that the aqueous phase has a small initial salinity and that any buildup in salinity caused by incorporation of H_2O into hydrate is rapidly dissipated into an unlimited reservoir of brine. Finally, the heat diffusion coefficient is about 500 times larger than the salinity transport coefficient, so we neglect the effect of heat transfer on limiting hydrate formation.

MODELING APPROACH

Stoichiometric Model for Hydrate Formation

The first key element of the model is a stoichiometric box model to predict the hydrate volume generated from a given amount of methane and water in a box of volume V_{tot} with fixed pressure and temperature. One important parameter to be used in the stoichiometric model is hydration number, N. Hydration number is defined as the number of aqueous phase molecules per guest gas phase molecule in the hydrate lattice. The hydration number for methane hydrate, $CH_4.NH_2O$, reported by different authors varies from 5 to 7 [6], [20]. In this paper hydration number is assumed to be 6.

Figure 1a shows a box filled with known initial volumes of methane and water, $V_{g,i}$ and $V_{w,i}$, and thus:

$$V_{g,i} + V_{w,i} = V_{tot} \qquad (1)$$

Suppose an increment of hydrate, δV_h, forms at the interface between gaseous and aqueous phase as the result of stoichiometric conversion of the corresponding increments of methane and water, δV_g and δV_w, (Figure 1b). Note that in this figure the volume of generated hydrate is less than the total volumes of the consumed methane and water, i.e. $\delta V = \delta V_g + \delta V_w - \delta V_h > 0$. In fact, hydrate formation would cause a volume reduction under temperature and pressure conditions typical of formations in nature. From this volume change emerge two different consequences depending on having a closed or open box. In both cases constant pressure is assumed, in keeping with the expected situation in nature.

For a closed system, where no fluid phase transport is allowed, the volume of the box must shrink to keep the pressure constant. In natural sediment, a “shrinking box” would correspond to sediment compaction which reduces porosity.

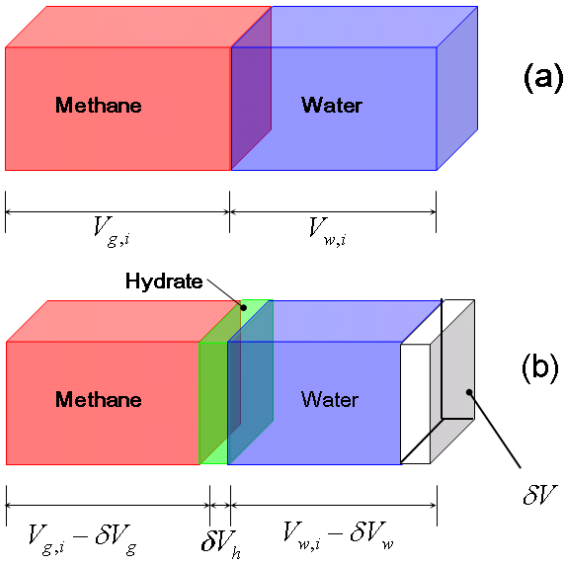

Figure 1- The box model to evaluate generated hydrate volume and associated volume change: (a) initial methane/water volumes, V_g and V_w, are fixed, and no hydrate is present initially. (b) An increment of hydrate, δV_h, forms at the interface between gas and water phases. δV shows the volume reduction due to the latter increment of hydrate.

Sediments in nature are expected to act as open systems, i.e. fluid phases can transport in/out, rather than closed systems. Therefore, an open box would be more appropriate to model natural situations. In the model of Figure 2, both water and methane are allowed to enter the box to compensate for the volume reduction during hydrate formation and thus maintain the pressure. Hydrate will keep forming until one or both of the components (methane, water) inside the box are fully consumed. We denote by R_n the ratio of number of gas phase moles, Δn_g, to the total number of moles of gas and aqueous phase, $\Delta n_g + \Delta n_w$, transported into the box. We let ΔV_g and ΔV_w denote the corresponding volumes of the gaseous phase and aqueous phase transported into the box. Two general cases can be considered in terms of the initial and transported amounts of water, $n_{w,i}$ and Δn_w, and methane, $n_{g,i}$ and Δn_g:

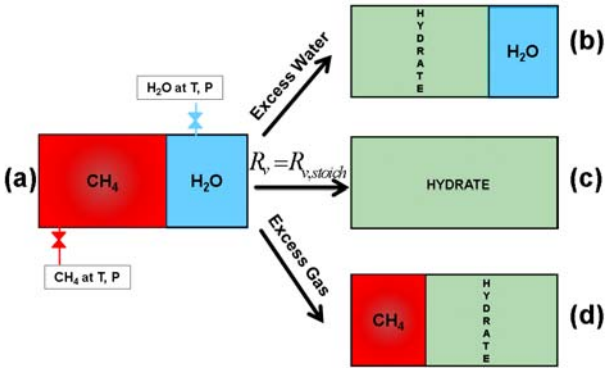

Figure 2- Final states of an open system (a) in which CH4 and H2O can enter during hydrate formation so that T, P are constant depend on how much of each phase enters. (b) total amount of water (initial amount + the amount entered) exceeds the stoichiometric requirement to convert the total gas; (c) the total amount of gas and water are at the exact stoichiometric ratio; (d) total amount

of gas (initial amount + amount entered) exceeds stoichiometric gas requirement to convert the total water.

I. Excess water: Total water exceeds stoichiometric requirement

Suppose that the total number of moles of water, $(n_{w,i} + \Delta n_w)$, is more than the stoichiometric amount of water required to convert the total amount of methane into hydrate, $N(n_{g,i} + \Delta n_g)$. Therefore, all the gas is consumed to form n_h moles of methane hydrate, which occupy a volume V_h.

$$n_h = \frac{V_h}{\bar{V}_h} = (n_{g,i} + \Delta n_g) = \frac{V_{g,i} + \Delta V_g}{\bar{V}_g} \qquad (2)$$

The final volume occupied by aqueous phase would be:

$$V_{w,f} = \bar{V}_w (n_{w,i} + \Delta n_w - N(n_{g,i} + \Delta n_g)) \qquad (3)$$

It can be shown [19] that the hydrate volume in terms of the value of $R_n = \frac{\Delta n_g}{\Delta n_w + \Delta n_g}$ is:

$$V_h = \frac{\bar{V}_h(\bar{V}_w + \bar{V}_g R_n - \bar{V}_w R_n)}{R_n(\bar{V}_h - \bar{V}_w) + \bar{V}_w - N\bar{V}_w R_n} n_{g,i} \qquad (4)$$

Figure 2b illustrates a typical final state of the system in the case of excess water. The volumes of fluid phases transported into the box can be expressed in terms of the initial volumes of gaseous and aqueous phases in the box and the final volume of hydrate:

$$\Delta V_w = V_{tot} - V_{w,i} + V_h(N\frac{\bar{V}_w}{\bar{V}_h} - 1) \qquad (5)$$

$$\Delta V_g = \frac{\bar{V}_g}{\bar{V}_h} V_h - V_{g,i} \qquad (6)$$

The total phase volume transported into the box, $\Delta V_w + \Delta V_g$, as a function of the final hydrate volume, V_h:

$$\Delta V_w + \Delta V_g = K_{trans} V_h \qquad (7)$$

wherein,

$$K_{trans} = \frac{N\bar{V}_w + \bar{V}_g}{\bar{V}_h} - 1 \qquad (8)$$

II. Excess methane: Total methane exceeds stoichiometric requirement

In this case, there is more methane than the required amount to convert the total amount of water into hydrate, i.e.:

$$n_{g,i} + \Delta n_g > \frac{1}{N}(n_{w,i} + \Delta n_w) \qquad (9)$$

Therefore, all the water is consumed to form n_h moles of methane hydrate:

$$n_h = \frac{V_h}{\bar{V}_h} = \frac{1}{N}(n_{w,i} + \Delta n_w) = \frac{1}{N}\frac{V_{w,i} + \Delta V_w}{\bar{V}_w} \qquad (10)$$

The final volume occupied by gas phase would be:

$$V_{g,f} = V_{g,i} + \Delta V_g - \underbrace{V_h \frac{\bar{V}_g}{\bar{V}_h}}_{Consumed\ CH_4} \qquad (11)$$

The final hydrate volume as a function of R_n in the excess methane case is given as:

$$V_h = \frac{\bar{V}_h(\bar{V}_w + \bar{V}_g R_n - \bar{V}_w R_n)}{(1-R_n)(\bar{V}_h - \bar{V}_g) + N\bar{V}_g R_n} n_{w,i} \qquad (12)$$

The total phase volume transported into the box, $\Delta V_w + \Delta V_g$, is governed by Eq. (7) regardless of having an excess water or excess methane case [19].

Figure 2c shows the special case where the final state of the system is having hydrate only. This special case occurs only if:

$$\frac{n_{w,i} + \Delta n_w}{n_{g,i} + \Delta n_g} = N \qquad (13)$$

It can be shown that

$$\Delta n_{g,stoich} = \frac{V_{tot}}{\bar{V}_h} - n_{g,i} \qquad (14)$$

Eqs. (13) and (14) give:

$$\Delta n_{w,stoich} = N\frac{V_{tot}}{\bar{V}_h} - n_{w,i} \qquad (15)$$

Therefore, the corresponding $R_n = R_{n,stoich}$ for this special case is calculated as:

$$R_{n,stoich} = \frac{\Delta n_{g,stoich}}{\Delta n_{g,stoich} + \Delta n_{w,stoich}} \qquad (16)$$

For a given initial phase content, $R_n < R_{n,stoich}$ represents an excess aqueous phase case while $R_n > R_{n,stoich}$ shows an excess gas case.

A volumetric ratio of gaseous phase entering the box is defined as:

$$R_v = \frac{\Delta V_g}{\Delta V_g + \Delta V_w} = \frac{\Delta n_g \bar{V}_g}{\Delta n_g \bar{V}_g + \Delta n_w \bar{V}_w} \qquad (17)$$

If only water phase enters to maintain pressure, then $R_v = 0$. If only gas phase enters, $R_v = 1$.

In order to extend the model to saturations in a volume of sediment, one pore volume of the sediment can be considered as the open box in the model, i.e. $V_{tot} = 1$ PV. Therefore, all the volumes ($V_{g,i}$, $V_{g,f}$, $V_{w,i}$, $V_{w,f}$ and V_h) can be replaced by the corresponding saturations ($S_{g,i}$, $S_{g,f}$, $S_{w,i}$, $S_{w,f}$ and S_h). Similarly, ΔV_w and ΔV_g may be replaced by dimensionless volumes, $\Delta V_{w,d}$ and $\Delta V_{g,d}$, in units of pore volume. For instance, Eq. (7) can be extended to calculate the total pore volumes of gas and aqueous phase transported into a sediment as in Eq. (18).

$$\Delta V_{g,d} + \Delta V_{w,d} = K_{trans} S_h \qquad (18)$$

Figure 3 shows S_h versus R_v for three different initial water saturations within a sediment under temperature and pressure of $T = 2^\circ\mathrm{C}$ and $P = 6.5\mathrm{MPa}$. Methane density was estimated to be $55\,\mathrm{kg/m^3}$ under the latter pressure and temperature. Water density and hydrate density was assumed $1000\mathrm{kg/m^3}$ (fresh water) and $914\frac{\mathrm{kg}}{\mathrm{m^3}}$, respectively. Each curve in Figure 3 passes through $S_h = 1$ when $R_v = R_{v,stoich}$. Regardless of the initial phase saturations, for values of $R_v < R_{v,stoich}$ the final state has only hydrate and water phases, i.e. excess water, and for $R_v > R_{v,stoich}$ the final state of the sediment is having hydrate and gas phase only, i.e. excess gas, [19].

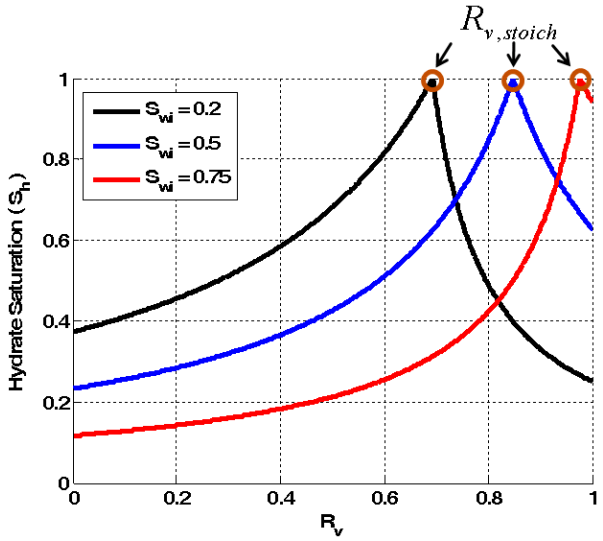

Figure 3- Hydrate saturation versus R_v for a sediment, into which methane and water can flow at a pressure of 6.5 MPa and temperature of $2^\circ\mathrm{C}$. Three initial methane/water saturations are considered. $R_{v,stoich}$ for each initial state of the sediment is shown with hollow circles.

Figure 4 shows transported methane, transported water and the total methane and water transported, calculated from Eq. (7), versus R_v for an initial water saturation of $S_{w,i} = 0.2$. Note that in the excess water case, the amount transported methane is a much stronger function of R_v compared to the amount of transported water which remains almost constant with R_v. In the excess methane case, both transported water and methane change sharply with R_v. An interesting point is that the total amount of fluid transported is in the order of one pore volume which is quite substantial.

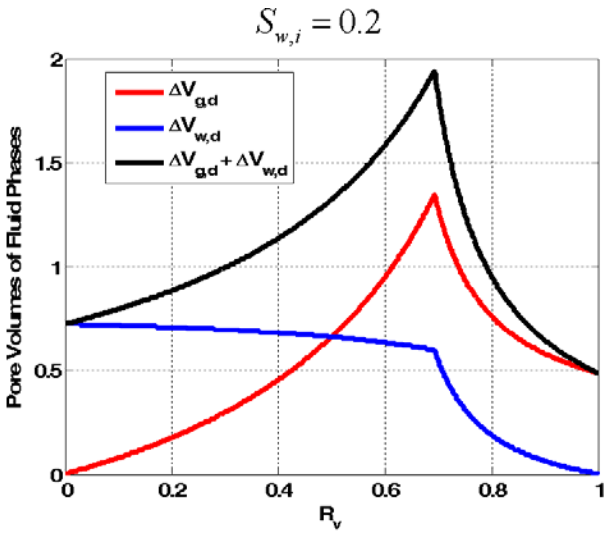

Figure 4- Transported methane, $\Delta V_{g,d}$, transported water, $\Delta V_{w,d}$, and total phase transported, $\Delta V_{g,d} + \Delta V_{w,d}$, during hydrate formation versus R_v for a sediment with initial water saturation of $S_{w,i} = 0.2$.

Effect of Volume Change during Hydrate Formation on Hydrate Saturation Profile

Hydrate formation in a thin layer of sediment within a column can be treated with the model of the preceding section. Therefore, having the initial gas saturation profile along a sediment column, the hydrate saturation profile resulting from moving the column into the GHSZ can be calculated.

Suppose a single gas column, disconnected from the original source of charge, has been established below a seal in sediment with known, uniform properties (i.e. grain size distribution). The BGHSZ is initially assumed to be at the top of the gas column and thus no hydrate initially exists in the sediment. Figure 5a illustrates such a gas column. As the BGHSZ descends through the gas column, methane and water above the BGHSZ start forming hydrate and thus the model introduced in the preceding section applies (Figure 5c).

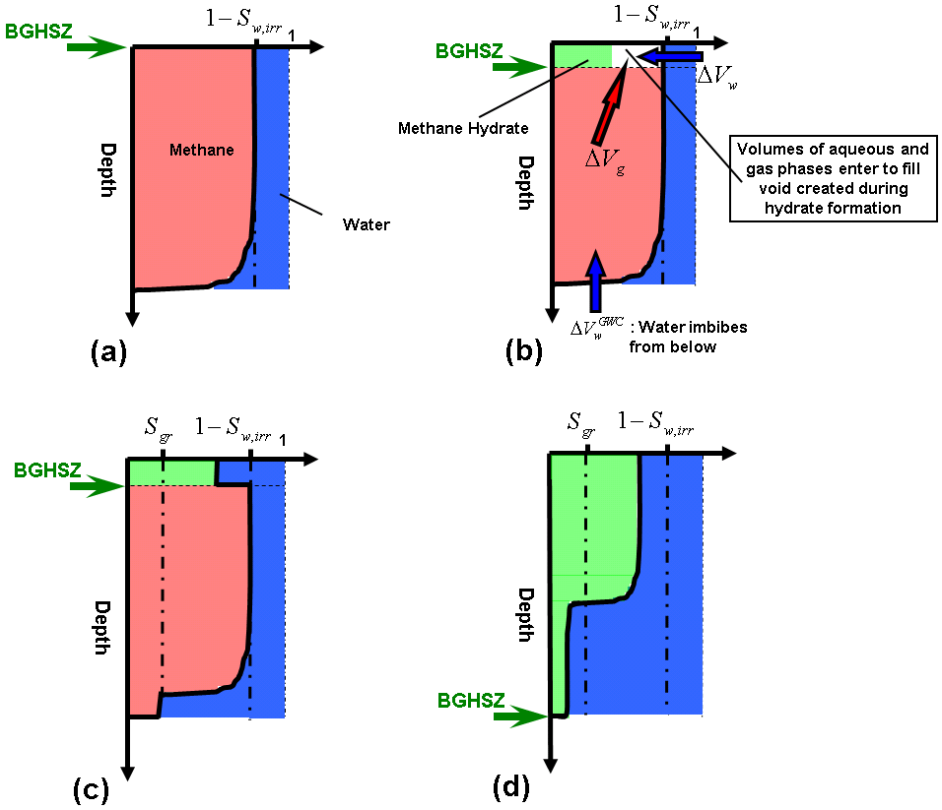

Figure 5-(a) A gas accumulation established in a homogeneous sediment which is below BGHSZ. (b) The state of the gas column after little descent of BGHSZ. The white area above the BGHSZ represents the volume change during hydrate formation. Water and methane transport into the HSZ to compensate for the volume reduction (c) More hydrate formed and the final hydrate saturation in the zone newly located in GHSZ can be estimated from the box model. (d) The final hydrate saturation after the BGHSZ has descended to the lowermost part of the gas column.

In Figure 5b red and blue arrows represent gas transport and water transport, respectively, to fill the void created by hydrate formation (cf. Eqs. 5 and 6). More hydrate is then formed from the transported methane. This will keep happening until the sediment section above the BGHSZ is filled with aqueous and hydrate phase (Figure 5c). Water must also imbibe from below to replace the transported methane. The water volume replacing gas is shown as ΔV_w^{GWC} on the figure. Consequently, the gas-water contact (GWC) rises and the gas saturation profile changes accordingly from the one shown in Figure 5a to that in Figure 5c.

After the BGHSZ has descended to the lowermost part of the gas column the hydrate saturation profile shows large saturations in the upper portion of the column and small saturations below (Figure 5d) which is qualitatively different from the initial gas saturation profile shown in Figure 5a [19].

RESULTS AND DISCUSSION

Applying the Model to Mt. Elbert Well

The model was applied to field data from Mt. Elbert gas hydrate stratigraphic test well [19]. The test well indicates two zones of large gas hydrate saturation (the D and C sand units) in the highest portions of the sands [18]. Besides, researchers have suggested that the gas hydrate deposits in Mt. Elbert well are free gas accumulations converted to hydrate after being placed in the GHSZ [21], [22]. Therefore, the proposed model was validated against data from Mt. Elbert well [19].

A prerequisite for the model is an estimate of capillary entry pressure versus depth [19]. This was estimated from grain size distribution at each depth [19]. Profiles of the 10^{th} and 50^{th} percentile of grain size in sand units D and C are shown in Figure 6a. The corresponding estimated capillary entry pressure profile is shown as dotted line in Figure 6b.

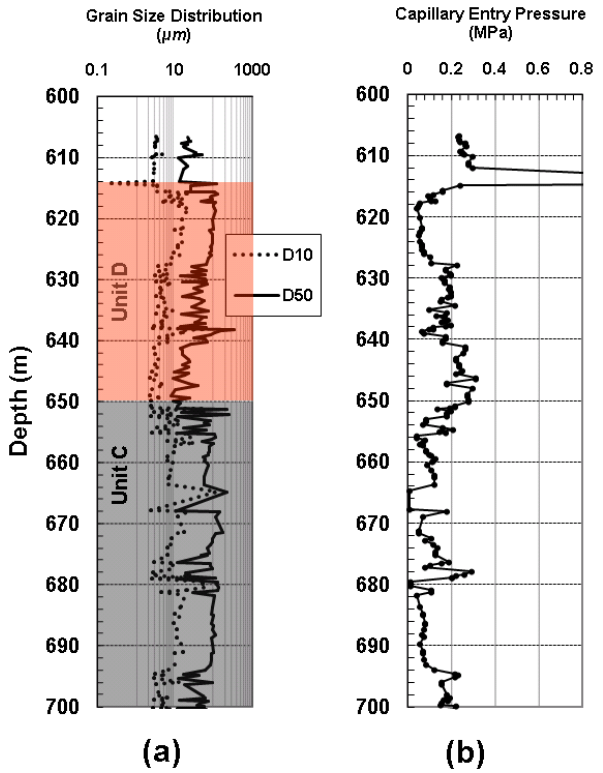

Figure 6-(a) D_{10} and D_{50} of grain size distribution versus depth in Mt. Elbert well. (b) Estimated capillary entry pressure (dotted line) [19]. Based on the capillary entry pressure profile, there is a strong seal at depth 614 m which is consistent with having a shaly layer at 614 m observed in Mt. Elbert well [23].

The gas accumulation was assumed to have been established between 614 m and 673 m and disconnected from the source of charge as in Figure 5. Figure 7a shows the estimated gas saturation profile (red solid line). The irreducible water saturation and the residual gas saturation was assumed to 20% and 30%, respectively [24], [25]. R_v is set as 0.55 throughout the sediment [19].

As the BGHSZ moves downward through the gas column, hydrate starts forming. As a result of volume reduction during hydrate formation some methane rises from lower

portions of the gas column. The transport of gas from lower portions to upper portions will be followed by the rise of GWC. Therefore, the capillary pressure is reduced throughout the gas column. Consequently, the capillary pressure falls below the capillary entry pressure at 650 m and thus the originally connected column of gas starts acting as two non-communicating gas columns, gas columns I and II, almost immediately after hydrate starts forming (Figure 7b).

Figure 7b shows the situation when the BGHSZ has moved about 3.5 meters downwards through the gas column. Based on the estimated initial gas saturation of 0.8 and a value of $R_v = 0.55$ the hydrate saturation is calculated to be 0.75 (Figure 3). The gas column comprises two disconnected regions labeled gas zone I and gas zone II (Figure 7b). Water has imbibed from below into the bottom 6 meters of gas zone I to compensate for the volume of gas that moved into the interval now containing hydrate. Gas zone II saturations remain essentially unchanged from their initial profile, because the disconnection from gas zone I occurred at the onset of hydrate formation.

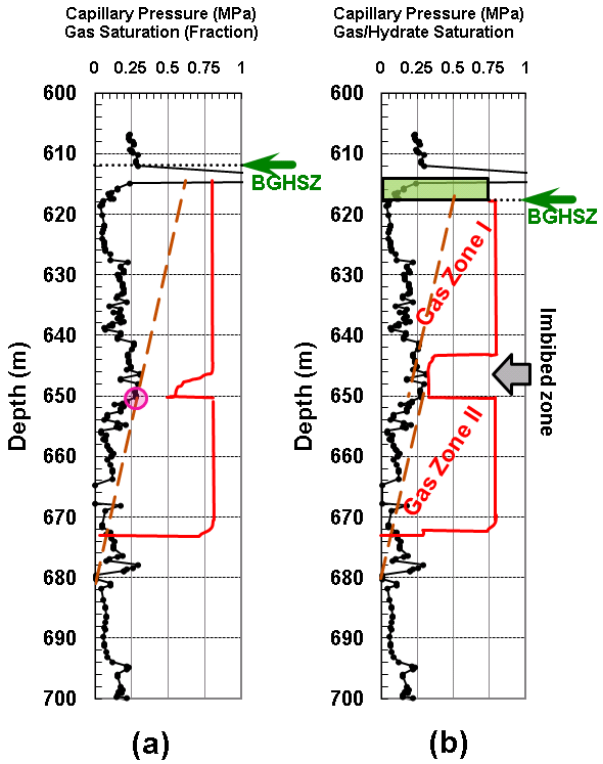

Figure 7- (a) Estimated initial gas saturation (red solid line) (b) Gas saturation profile (red) when BGHSZ has moved 3.5 meters downward through the gas column. The resulting hydrate saturation is shown as green fill. $R_v = 0.55$ is used in the model to calculate the hydrate saturation. Aqueous phase has imbibed into gas zone I from below to compensate for the gas phase migration to the hydrate zone. Gas zones I and II are no longer communicating due to the capillary barrier at 650 m.

Figure 8 shows the final hydrate saturation profile once the BGHSZ has moved all the way to the bottom of the gas column. During hydrate formation in the imbibed portions of gas column, only aqueous phase moves to compensate for the void space due to hydrate formation, i.e. $R_v = 0$. Therefore, the model predicts large hydrate saturations of 0.75 in the upper portions of sand units C and D, and small hydrate saturations of 0.13 in the lower portions [19].

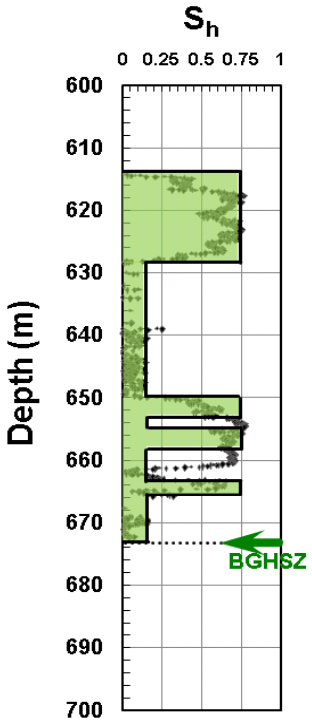

Figure 8- Final hydrate saturation profile predicted by the model [19]. The log derived hydrate saturations are shown as dots [26].

Comparing the Model Prediction with Log-Derived Observations

Assuming $R_v = 0.55$ yields a very good match with the log-derived hydrate saturation profile in unit D. This value of R_v underestimated the thickness of the portion with large hydrate saturation in unit C. The log-derived data suggest highly variable but small hydrate saturation in parts of the lower portions of units C and D. The model predicts a uniform, small saturation of hydrate there, about 13% in the depth ranges of 628-650, 653.5-655, 658-664 and 666-673 meters [19]. The model prediction is consistent with the nonzero but small hydrate saturations predicted from pore fluid geochemistry analysis [27].

Volume of Fluid Phases Transported into the Hydrate-Bearing Zone

The total transported pore volumes of fluid changes linearly with the final hydrate saturation, Eq. (7), with a slope of $K_{trans} \approx 1.9$ for the assumed P and T in Mt. Elbert. The amount of fluid phases transported into the hydrate-bearing zone is substantial, around 1.4 pore volumes in the upper portions of units C and D in Mt Elbert (Figure 9). Even in the portions of small hydrate saturation in each sand unit, about 0.3 PV of aqueous phase would have moved into the GHSZ. In addition to that, $\Delta V_{w,d}^{GWC} = 0.5$ PV of water has been transported to replace gas in the imbibed zone. Therefore a total of 0.8 PV of water has been transported into the imbibed zones, with low hydrate saturations, during hydrate formation.

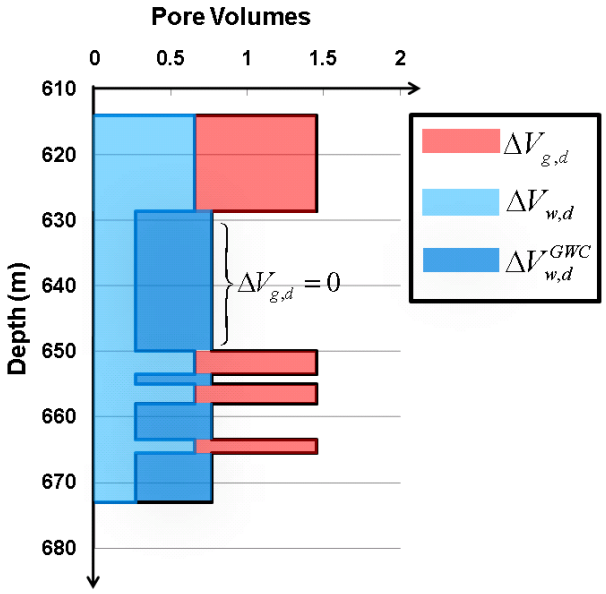

Figure 9- Considerable volume of fluid (red: gas phase; blue: aqueous phase) must be transported into the hydrate-bearing zone in Mt. Elbert well if the hydrate formed from a pre-existing gas accumulation. Note that this is in addition to the one pore volume of sediment which is initially filled with aqueous and gas phase.

Can Co-current Flow Provide Fluids to the Hydrate Zone?

The conversion of methane and water to hydrate reduces the volume occupied by the fluid phases, and this will cause the local fluid pressure to decrease. Hence a gradient in fluid pressure will arise when hydrate formation begins. We now consider how this gradient could move the needed fluid volumes to the GHSZ. Because the model assumes the gas accumulation is no longer connected to the source of the gas charge, the gaseous phase must flow upwards within the accumulation toward the BGHSZ. It is of interest then to consider whether the aqueous phase can flow cocurrently with the gas.

For our one-dimensional (vertical) model, Darcy's law for the aqueous phase is given by

$$u_w = \frac{-kk_{r,w}}{\mu_w}\frac{\partial}{\partial z}(P_w + \rho_w g z) \qquad (19)$$

And thus:

$$u_w = \frac{-kk_{r,w}}{\mu_w}(\frac{\partial P_w}{\partial z} + \rho_w g) \qquad (20)$$

Here u_w is the Darcy velocity of aqueous phase, μ_w is the viscosity of aqueous phase, $k_{r,w}$ is the relative permeability of the sediment to the aqueous phase and P_w denotes the pressure in the aqueous phase. g is the acceleration due to gravity.

Similarly, for the gaseous phase Darcy's law is given by

$$u_g = \frac{-kk_{r,g}}{\mu_g}(\frac{\partial P_g}{\partial z} + \rho_g g) \qquad (21)$$

P_g and P_w are related through the following equation:

$$P_g - P_w = P_c(z) = (\rho_w - \rho_g)g(z - z_0) \quad (22)$$

where $P_c(z)$ is capillary pressure as a function of depth, z. z_0 is the depth of the free water level at which the capillary pressure is zero.

Combining Eqs. (21) and (22) gives:

$$u_g = \frac{-kk_{r,g}}{\mu_g}\left(\frac{\partial P_w}{\partial z} + \frac{\partial P_c}{\partial z} + \rho_g g\right) \quad (23)$$

Eq. (22) also gives that:

$$\frac{\partial P_c}{\partial z} = (\rho_w - \rho_g)g \quad (24)$$

Eqs. (23) and (24) gives:

$$u_g = \frac{-kk_{r,g}}{\mu_g}\left(\frac{\partial P_w}{\partial z} + \rho_w g\right) \quad (25)$$

Therefore, for cocurrent flow

$$\frac{q_g}{q_w} = \frac{u_g}{u_w} = \frac{\lambda_g}{\lambda_w} \quad (26)$$

Here q_g and q_w are the volumetric flow rate of the gaseous and aqueous phases, respectively. λ_g and λ_w are effective mobility of gaseous and aqueous phases, respectively. Mobility of a phase, *p*, is defined as $\lambda_p = \frac{kk_{r,p}}{\mu_p}$; $p = g, w$.

Hence:

$$R_v = \frac{\Delta V_g}{\Delta V_g + \Delta V_w} = \frac{q_g}{q_g + q_w} = \frac{\lambda_g}{\lambda_g + \lambda_w} \quad (27)$$

In other words, the assumption of cocurrent flow leads to identifying R_v as the fractional flow of the gaseous phase. This provides an independent constraint on the value of R_v that could have occurred during hydrate formation. Interestingly, this constraint is independent of the magnitude of the pressure gradient induced by hydrate formation and independent of the permeability of the sediment.

Dynamic methane viscosity, μ_g, is estimated to be $\approx 1.2 \times 10^{-5}$ Pa.s at $P = 6.5$ MPa and a $T = 2^{\circ}$C [28]. At the same thermodynamic condition, viscosity of water, μ_w, is estimated to be $\approx 1.7 \times 10^{-3}$ Pa.s [29].

Figure 10a shows a typical relative permeability curve for water wet granular media. Note that the residual gas saturation, $S_{g,r}$, is 0.3 and the irreducible wetting phase saturation, $S_{w,irr}$, is 0.2. Thus from Eq. (27) we calculate the value of R_v for a range of values of water saturation at which gas and aqueous phases are assumed to be flowing. The results are shown in Figure 10b.

Figure 11 is similar to Fig. 3 but with different values of initial water saturation. Suppose for illustration that cocurrent flow occurs at the same saturation as the initial state. Consider two values of initial water saturations S_{wi} = 0.4 and S_{wi} = 0.6, marked as a

solid star and a solid circle, on Figure 10b. The corresponding values of R_v are close to unity, Fig 10b, and lead to final states in which hydrate and gas phases coexist. These states are shown with the same symbols on Figure 11a and Figure 11b. Repeating this calculation for the full range of initial saturations yields the curve of Figure 11b. The zones of excess methane (final state is hydrate and gas phases) and excess water (final state is hydrate and aqueous phases) are shown in red fill and blue fill, respectively.

Therefore, if we assume that the water and methane required during hydrate formation, $\Delta V_{w,d}$ and $\Delta V_{g,d}$, are provided through a co-current flow at the same saturation state as the initial gas accumulation, the sediment would be hydrate and methane only (excess methane) for a rather large range of initial water saturations, i.e. $S_{w,i} < 0.62$ for the typical relative permeability curve in Figure 10a. The latter is in contradiction to the observed current situation in Mt. Elbert well of only hydrate and aqueous phase saturations [26]. Figure 11b further shows that the observed state of the Mount Elbert well would arise only over a very narrow range of initial water saturation. This range corresponds to rather small initial gas saturations, $S_{g,i} < 0.4$. The capillary entry pressure estimations predict a much larger initial gas saturation (Figure 7a). Therefore, we conclude that it is unlikely that cocurrent flow took place without changing the initial saturations.

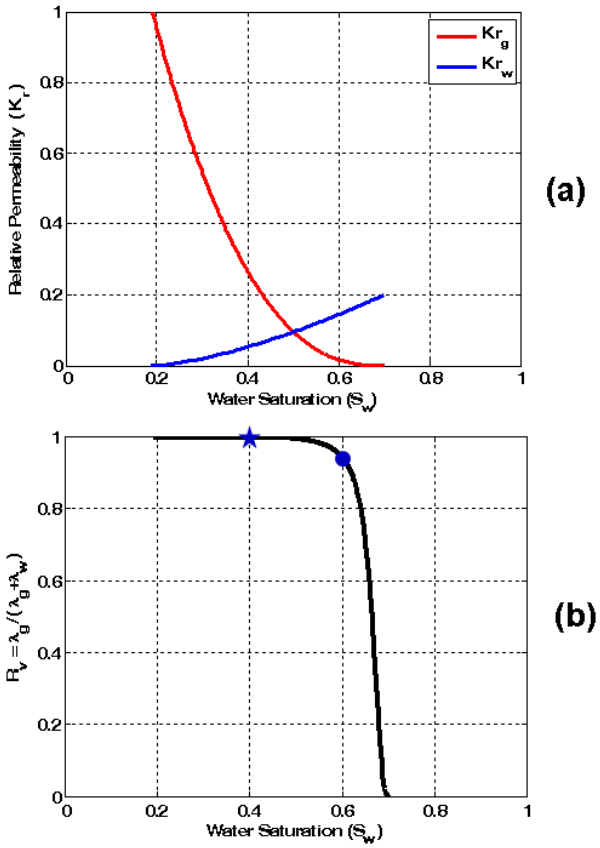

Figure 10-Assuming cocurrent vertical flow of gas and aqueous phases allows estimating R_v in terms of phase mobilities. (a) A typical relative permeability curve; red represents the relative permeability

of gaseous phase and blue represents that of the wetting phase. (b) R_v versus water saturation at which cocurrent flow occurs calculated from Eq. (27).

To constrain the saturation at which cocurrent flow might have occurred, we apply classical fractional flow theory [30]. Figure 12 shows the fractional flow of the aqueous phase corresponding to the relative permeability curves shown in Figure 10a. As indicated in Figure 13, the downstream boundary condition in the gas column is $S_w = S_{w,i}$ while the upstream boundary condition is $f_w = 1$. The latter corresponds to aqueous phase entering the sediment to raise the GWC. These boundary conditions give rise to an upward moving front at which a step change in saturation occurs, Figure 13. The water saturation at the front can be determined graphically by drawing a tangent from the initial saturation point to the $f_w(S_w)$ curve. The tangent lines for three values of initial saturation ($S_{w,i} = 0.2$, 0.4 and 0.6) are drawn on the fractional flow curve shown in Figure 12.

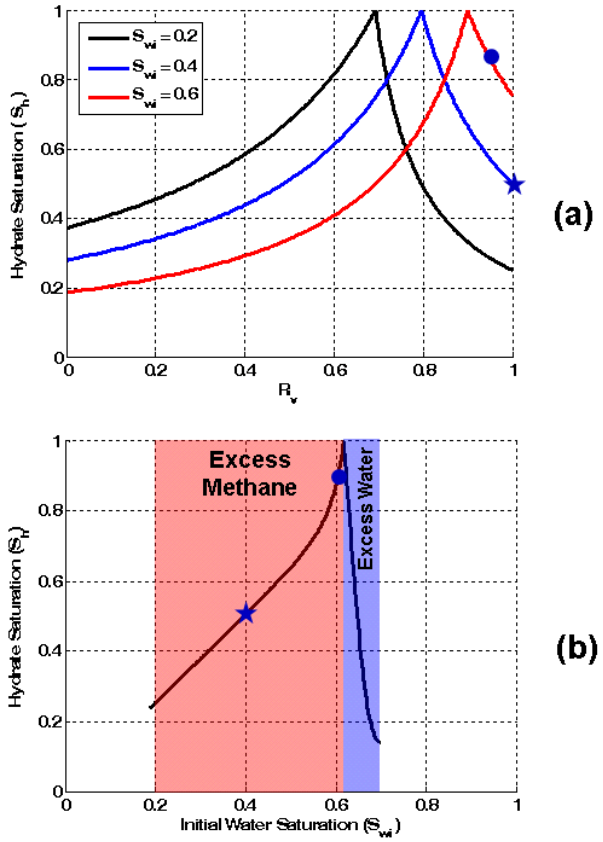

Figure 11-Calculating hydrate saturation, S_h, from initial water saturation, $S_{w,i}$ and R_v, assuming co-current flow at the initial saturation. (a) Hydrate saturation versus R_v for different initial water saturations. The points corresponding to the two arbitrary water saturations, marked as a solid star and a solid circle, on Figure 10b are shown with the same symbols. (b) Hydrate saturation versus initial and flowing water saturation constructed through combining Figure 10b and Figure 11a.

Based on the tangent lines in Figure 12, the front saturation, $S_{w,front}$, would be almost the same for all three initial water saturations: $S_{w,front} \approx 1 - S_{gr} = 0.7$. Corresponding fractional flow of aqueous phase would be $f_{w,front} \approx 1$. Ahead of the front, the water saturation is $S_w = S_{w,i}$ and $f_w \approx 0$. Thus only gas is arriving ($f_g \approx 1$) at the BGHSZ. This situation is expected for almost any set of relative permeability curves because the viscosity ratio dominates the mobility ratio, forcing λ_w / λ_g to be very small. Consequently, the displacement becomes piston type, where water pushes gas ahead in a piston type manner. This piston type movement of a methane bank ahead of the water bank can provide the upper zones in which hydrate is forming with the needed gas $\Delta V_{g,d}$. Simultaneously this piston type movement of aqueous phase would enable the transport of water, $\Delta V_{w,d}^{GWC}$, to replace transported gas from below and raise the GWC. But clearly the cocurrent flow cannot have transported water into the zone of hydrate formation

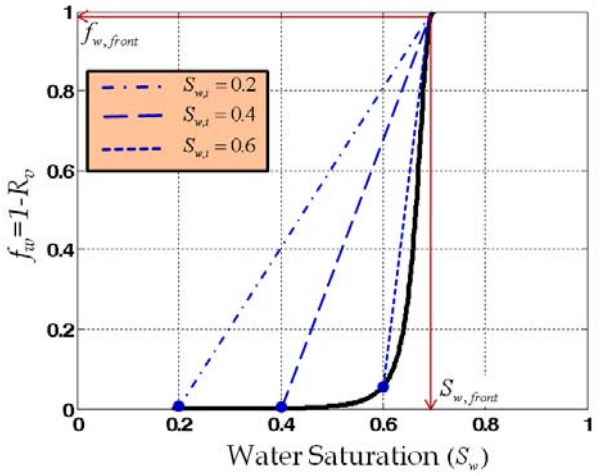

Figure 12- Fractional flow of a co-current flow of methane and water. The shock front (tangent lines) determines a piston type movement with $S_{w,front} \approx 1 - S_{gr}$ regardless of the initial water saturation.

The need for considerable amount of water, $\Delta V_{w,d}$, during hydrate formation suggests another route for water flow: water moves down through accumulated hydrate from the unfrozen water above (Figure 13). For this to happen the water phase must remain connected within the hydrate-bearing sediment. This requires the final hydrate saturation at the upper zones to be less than $1 - S_{w,irr}$ so the aqueous phase is connected at the final water saturation. The model described above predicts that this condition will arise, because imbibition occurs in the upper zones as the GWC rises.

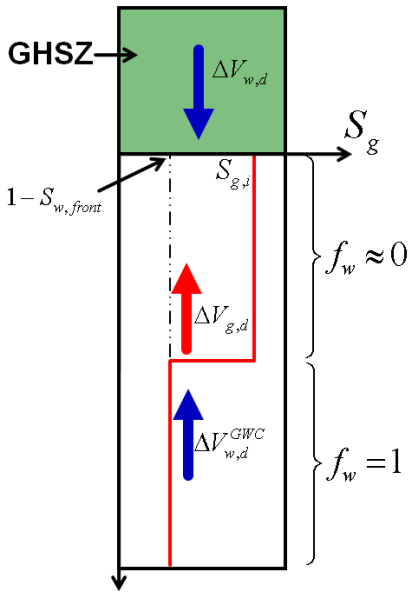

Figure 13- Model for the transported volumes of aqueous and gas phase. Fractional flow theory proves it unlikely that the required amount of aqueous phase, $\Delta V_{w,d}$, has been transported through a co-current flow with the gas phase.

CONCLUSION

Analysis shows that considerable amount of fluid (gaseous and aqueous phase) needs to be transported during hydrate formation. Moreover, fractional flow theory shows that due to the very low mobility ratio of aqueous to gas phase, the amount of water required during hydrate formation, $\Delta V_{w,d}$, cannot be transported through a co-current type of flow.

It is rather another type of flow, i.e. water is transported from above into the hydrate formation zone and gas is being provided from the lower free gas column. In our future work we will examine the constraints that must be satisfied in order for this much water to move through the hydrate-bearing sediment.

NOMENCLATURE

D_{10} 10th percentile of grain size distribution (L)

D_{50} 50th percentile of grain size distribution (L)

D_{60} 60th percentile of grain size distribution (L)

g Gravitational acceleration

K Hydraulic conductivity (LT^{-1})

k Permeability (L^2)

$k_{r,w}$ Relative permeability to aqueous phase (dimensionless)

$k_{r,g}$ Relative permeability to gaseous phase (dimensionless)

MW_g Molecular weight of methane (M/M)

MW_h Molecular weight of hydrate (M/M)

MW_w Molecular weight of water (M/M)

$n_{g,i}$ Initial number of moles of methane (M)

$n_{w,i}$ Initial number of moles of water (M)

$P_{c,entry}$ Capillary entry pressure ($ML^{-1}T^{-2}$)

P_g Pressure in the gas phase ($ML^{-1}T^{-2}$)

P_w Pressure in the aqueous phase ($ML^{-1}T^{-2}$)

q_g Volumetric flow rate of gaseous phase (L^3T^{-1})

q_w Volumetric flow rate of aqueous phase (L^3T^{-1})

r_{avg} Average radius (L)

r_{eq} Equivalent radius (L)

R_n Molar ratio of transported gas phase (dimensionless)

R_v Volume ratio of transported gas phase (dimensionless)

S_g Gas phase saturation (dimensionless)

S_h Hydrate phase saturation (dimensionless)

S_w Aqueous phase saturation (dimensionless)

U Coefficient of uniformity (dimensionless)

u_g Darcy velocity of gaseous phase (LT^{-1})

u_w Darcy velocity of aqueous phase (LT^{-1})

$V_{m,g}$ Molar volume of methane (L^3/M)

$V_{m,h}$ Molar volume of hydrate (L^3/M)

$V_{m,w}$ Molar volume of water (L^3/M)

ρ_g Methane density (ML^{-3})

ρ_h Hydrate density (ML^{-3})

ρ_w Water density (ML^{-3})

σ Interfacial tension (MT^{-2})

λ_g Effective mobility to gaseous phase

λ_w Effective mobility to aqueous phase

μ Viscosity ($ML^{-1}T^{-1}$)

ΔV_g Volume of transported aqueous phase (L^3)

ΔV_w Volume of transported aqueous phase (L^3)

$\Delta V_{g,d}$ Dimensionless volume of transported aqueous phase (pore volumes)

$\Delta V_{w,d}$ Dimensionless volume of transported aqueous phase (pore volumes)

REFERENCES

[1] N. V. Cherskii and é A. Bondarev, "Thermal method of developing gas-hydrate deposits," *Doklady Akademii Nauk SSSR*, vol. 203, p. 550, 1972.

[2] E. Sloan, *Clathrate hydrates of natural gases*, 2nd ed. New York: Marcel Dekker, 1998.

[3] T. S. Collett, “Potential of gas hydrates outlined,” *The Oil and Gas Journal*, vol. 90, no. 25, p. 84, Jun. 1992.
[4] Y. P. Handa and D. Y. Stupin, “Thermodynamic properties and dissociation characteristics of methane and propane hydrates in 70-.ANG.-radius silica gel pores,” *The Journal of Physical Chemistry*, vol. 96, no. 21, pp. 8599-8603, Oct. 1992.
[5] V. Melnikov and A. Nestero, “Modeling of gas hydrates formation in porous media,” presented at the Second International Conference on Natural Gas Hydrates, United Engineering Foundation, Toulouse, France, 1996.
[6] A. W. Rempel and B. A. Buffett, “Formation and accumulation of gas hydrate in porous media,” *Journal of Geophysical Research*, vol. 102, no. 5, pp. 10151-10164, 1997.
[7] B. M. Clennell, M. Hovland, J. S. Booth, P. Henry, and W. J. Winters, “Formation of natural gas hydrates in marine sediments 1. Conceptual model of gas hydrate growth conditioned by host sediment properties,” *Journal of Geophysical Research*, vol. 104, no. 10, pp. 22985-23003, 1999.
[8] G. D. Ginsburg, “Gas hydrate accumulation in deep-water marine sediments,” *Geological Society, London, Special Publications*, vol. 137, no. 1, pp. 51-62, Jan. 1998.
[9] B. Buffett, “Formation of gas hydrate from dissolved gas in natural porous media,” *Marine Geology*, vol. 164, no. 1-2, pp. 69-77, Feb. 2000.
[10] C. Hensen and K. Wallmann, “Methane formation at Costa Rica continental margin—constraints for gas hydrate inventories and cross-décollement fluid flow,” *Earth and Planetary Science Letters*, vol. 236, no. 1-2, pp. 41-60, Jul. 2005.
[11] G. Bhatnagar, W. G. Chapman, G. R. Dickens, B. Dugan, and G. J. Hirasaki, “Generalization of gas hydrate distribution and saturation in marine sediments by scaling of thermodynamic and transport processes,” *American Journal of Science*, vol. 307, no. 6, pp. 861-900, Jun. 2007.
[12] G. Bhatnagar, W. G. Chapman, G. R. Dickens, B. Dugan, and G. J. Hirasaki, “Sulfate-methane transition as a proxy for average methane hydrate saturation in marine sediments,” *Geophysical Research Letters*, vol. 35, no. 3, Feb. 2008.
[13] J. Phirani, R. Pitchumani, and K. Mohanty, “Transport Properties of Hydrate Bearing Formations from Pore-Scale Modeling,” in *Proceedings of SPE Annual Technical Conference and Exhibition*, 2009.
[14] M. E. Torres, K. Wallmann, A. M. Tréhu, G. Bohrmann, W. S. Borowski, and H. Tomaru, “Gas hydrate growth, methane transport, and chloride enrichment at the southern summit of Hydrate Ridge, Cascadia margin off Oregon,” *Earth and Planetary Science Letters*, vol. 226, no. 1-2, pp. 225-241, Sep. 2004.
[15] X. Liu and P. Flemings, “Passing gas through the hydrate stability zone at southern Hydrate Ridge, offshore Oregon,” *Earth and Planetary Science Letters*, vol. 241, no. 1-2, pp. 211-226, Jan. 2006.
[16] X. Liu and P. B. Flemings, “Dynamic multiphase flow model of hydrate formation in marine sediments,” *Journal of Geophysical Research*, vol. 112, no. 3, Mar. 2007.
[17] J. Behseresht, Y. Peng, M. Prodanovic, S. Bryant, A. Jain, and R. Juanes, “Mechanisms by Which Methane Gas and Methane Hydrate Coexist In Ocean Sediments,” in *Proceedings of Offshore Technology Conference*, 2008.
[18] R. Boswell et al., “Geologic controls on gas hydrate occurrence in the Mount Elbert prospect: Milne Point Unit, Alaska North Slope,” *Marine and Petroleum Geology*, Dec. 2009.
[19] J. Behseresht and S. L. Bryant, “Sedimentological Control on Saturation Distribution in Arctic Gas-Hydrate-Bearing Sands,” *submitted,*, 2011.
[20] V. P. Voronov, E. E. Gorodetskii, and S. S. Safonov, “Thermodynamic Properties of Methane Hydrate in Quartz Powder,” *The Journal of Physical Chemistry B*, vol. 111, no. 39, pp. 11486-11496, Oct. 2007.

[21] T. S. Collett, “Natural Gas Hydrates of the Prudhoe Bay and Kuparuk River Area, North Slope, Alaska,” *AAPG Bulletin*, vol. 77, no. 5, p. 793, 1993.
[22] T. Collett, “Energy resource potential of natural gas hydrates,” *AAPG Bulletin*, vol. 86, no. 11, pp. 1971-1992, 2002.
[23] K. Rose, R. Boswell, and T. Collett, “Mount Elbert Gas Hydrate Stratigraphic Test Well, Alaska North Slope: Coring operations, core sedimentology, and lithostratigraphy,” *Marine and Petroleum Geology*, vol. 28, no. 2, pp. 311-331, Feb. 2011.
[24] Y. Peng, M. Prodanovic, and S. L. Bryant, “Improving Fidelity of Network Models for Drainage and Imbibition,” in *Proceedings of SPE Annual Technical Conference and Exhibition*, 2009.
[25] J. Behseresht, S. L. Bryant, and K. Sepehrnoori, “Infinite-Acting Physically Representative Networks for Capillarity-Controlled Displacements,” *SPE Journal*, vol. 14, no. 4, pp. 568-578, 2009.
[26] M. W. Lee and T. Collett, “In-situ gas hydrate hydrate saturation estimated from various well logs at the Mount Elbert Gas Hydrate Stratigraphic Test Well, Alaska North Slope,” *Marine and Petroleum Geology*, vol. 28, no. 2, pp. 439-449, Feb. 2011.
[27] M. E. Torres, T. Collett, K. Rose, J. C. Sample, W. Agena, and E. Rosenbaum, “Pore fluid geochemistry from the Mount Elbert gas hydrate stratigraphic test well, Alaska North Slope,” *Marine and Petroleum Geology*, Oct. 2009.
[28] E. T. S. Huang, G. W. Swift, and F. Kurata, “Viscosities of methane and propane at low temperatures and high pressures,” *AIChE Journal*, vol. 12, no. 5, pp. 932-936, Sep. 1966.
[29] E. M. Stanley and R. C. Batten, “Viscosity of water at high pressures and moderate temperatures,” *The Journal of Physical Chemistry*, vol. 73, no. 5, pp. 1187-1191, May. 1969.
[30] S. E. Buckley and M. C. Leverett, “Mechanism of fluid displacement in sands,” *Petroleum Transactions, AIME*, vol. 146, pp. 107-116, 1942.

National Energy Technology Laboratory

626 Cochrans Mill Road
P.O. Box 10940
Pittsburgh, PA 15236-0940

3610 Collins Ferry Road
P.O. Box 880
Morgantown, WV 26507-0880

13131 Dairy Ashford, Suite 225
Sugarland, TX 77478

1450 Queen Avenue SW
Albany, OR 97321-2198

2175 University Ave. South
Suite 201
Fairbanks, AK 99709

Visit the NETL website at:
www.netl.doe.gov

Customer Service:
1-800-553-7681